Chemical Engineering & Processing: Process Intensification 198 (2024) 109715

Contents lists available at ScienceDirect

Chemical Engineering and Processing - Process Intensification

journal homepage: www.elsevier.com/locate/cep

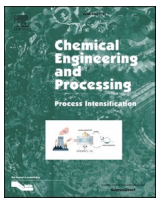

Importance of design and operating parameters in a sonication system for viscous solutions: effects of input power, horn tip diameter and reactor capacity

Ariana Bampouli [a,1], Quinten Goris [a,1], Mohammed Noorul Hussain [a,2], Olivier Louisnard [b], Georgios D. Stefanidis [c], Tom Van Gerven [a,*]

[a] Department of Chemical Engineering, Process Engineering for Sustainable Systems, KU Leuven, Celestijnenlaan 200F, 3001 Heverlee, Belgium
[b] Centre RAPSODEE, IMT Mines-Albi, UMR CNRS 5302, Université de Toulouse, Albi CT, France
[c] School of Chemical Engineering, Department of Process Analysis and Plant Design, National Technical University of Athens, Iroon Polytecneiou 9, Zografou 15780, Athens, Greece

ARTICLE INFO

KEYWORDS:
Cavitation
Liquid properties
Viscosity effect
Calorimetry
Sonochemiluminescence

ABSTRACT

This study investigates the distribution of ultrasound (US) energy in a batch system for solutions with viscosity ranging from 1 to approximately 3000 mPas. Sonication was performed using horn type configurations operating at 20-30 kHz and rated power capacity of 50 or 200 W. Two different tip diameters (3 or 7 mm) and two insertion depths (35 or 25 mm) within vessels of different sizes (≈60 or 130 ml) were utilized. Additionally, a special conical tip design was employed. For each experimental setup, the calorimetric efficiency was estimated, the cavitationally active regions were visualized using the sonochemiluminescence (SCL) method and bubble cluster formation inside the vessel was macroscopically observed using a high speed camera (HSC). In the viscosity range tested, the calorimetry results showed that the efficiency and continuous operation of the device depend on both the rated power and the horn tip diameter. The ratio between electrical and calorimetric power input remained consistently around 40 to 50% across the different configurations for water, but for the 123.2 mPas solution exhibited significant variation ranging from 40 to 85%. Moreover, the power density in the smaller reactor was found to be nearly double compared to the larger one. The SCL analysis showed multiple cavitationally active zones in all setups, and the zones intensity decreased considerably with increase of the solutions viscosity. The results for the cone tip were not conclusive, but can be used as the basis for further investigation. The current research highlights the importance of thoroughly understanding the impact of each design parameter, and of establishing characterization methodologies to assist in the future development of scaled-up, commercial applications.

1. Introduction

The application of ultrasound (US) energy can accelerate reaction activation, potentially leading to faster synthesis of desired chemical compounds [1]. Moreover, under appropriate conditions, sonication can even lead to the formation of new, unexpected chemical species [1]. Examples of US assisted processes include synthesis, crystallization and separation for fine chemicals and pharmaceuticals production [2–6] as well as routes to bulk products, such as polymerization. The majority of literature concerning ultrasound-assisted polymers production focuses on chain-growth reactions initiated by free radicals, such as in the cases of polystyrene and polymethyl methacrylate [7–9]. On the contrary, there is a notable scarcity of examples related to step-growth polymerizations such as the case of polyurethanes, despite their industrial significance [10].

As ultrasound waves propagate through a medium, they impart energy that can cause deviation of the system from its equilibrium state, leading to perturbations in pressure and temperature [1]. During the transmission of the US waves, the alternation of compressions and rarefactions along the direction the wave travels can lead to the formation

* Corresponding author.
E-mail address: tom.vangerven@kuleuven.be (T. Van Gerven).
[1] A. Bampouli and Q. Goris contributed equally to the work.
[2] Current address: Department of Physics, University of Antwerp, Groenenborgerlaan 171, 2020 Antwerp, Belgium.

https://doi.org/10.1016/j.cep.2024.109715
Received 23 October 2023; Received in revised form 12 February 2024; Accepted 19 February 2024
Available online 21 February 2024

of gas-filled microbubbles due to negative pressure [1,11]. The bubble formation, growth, and eventual violent collapse is known as acoustic cavitation [11,12]. Furthermore, due to the unequal pressure distribution in the liquid medium, a mean net fluid flow is created, termed acoustic streaming [13–15]. Due to the combined effects of acoustic cavitation and acoustic streaming, sonication can cause both chemical changes through the generation of radical species as well as mechanical effects by applying shear stresses that act upon the bulk medium layers [12,16]. Additionally, an increase in micromixing has been reported, even for viscous solutions [17,18].

Experimental investigations of these sonochemical effects can be conducted using techniques such as calorimetry [18,19], acoustic pressure measurements [20,21] and sonoluminescence or sonochemiluminescence (SCL) [19,22] methods. Alternatively, numerical simulations can be employed to predict the distribution of acoustic energy in the system [2,23,24]. A comprehensive overview of the most commonly applied procedures to investigate the sonochemical activity within a system is presented in several works [12,25]. Each characterization technique provides different information and encounters specific challenges and limitations [12,25]. Therefore, it might be advisable to combine several techniques to gain a complete understanding of the sonochemical effects in an ultrasound reactor [25]. For instance, calorimetric or chemical dosimetry methods yield integral information on the reactor performance, which can be used to quantitatively compare different sonication setups. On the downside, sub-optimal reactor performance cannot be explained, since no visualization of the sonochemical active zones can be achieved. Concurrently, SCL can be used to map the cavitation zones but does not directly provide quantitative information on the sonochemical performance of the system.

In most cases, the initial stage in the design of a sonochemical system involves the preparation of an elaborate experimental campaign conducted in laboratory-scale vessels [12,25–27]. This step is essential for gaining insights into the system. Nevertheless, due to the non-uniform distribution of cavitation in a sonochemical reactor, experimental campaigns remain necessary even on pilot scale [28,29]. Baths, probes, and Langevin transducers are the most commonly employed devices for the sonication of a mixture. The advantages and drawbacks of using each type of apparatus have been covered in depth in the literature [25,30,31]. Ultrasonic probes (called horns or sonotrodes for simplicity) are used in a considerable part of the sonochemistry related literature [10,32–34]. The operation principle of ultrasonic horns is based on the vibrational movement of the tip of the shaft within the liquid, with a displacement amplitude ranging from a few to several micrometers. However, it is worth noting that a larger amplitude does not necessarily lead to increased cavitation activity [34]. At the same time, the selection of the precise elements for the design of a sonication system is a non-trivial process. Several factors must be considered, including the solution properties [31,32,35,36], the frequency [22,28,29,37] and power of sonication [31,38], the sonication duration, the US processing mode (continuous or pulsed) [39], the temperature of the bulk [31,36], and the reactor design [22,28,29,31], among others. Consideration of these factors is important for the optimization of the efficiency and consistency of the sonication process [12,25,40].

As previously mentioned, research has shown that sonication offers significant benefits in the processing of high viscosity products such as polymers [7,9]. In these cases, the viscosity of the solution is one of the most critical physicochemical properties [7,31,35,41] determining the efficacy of the sonochemical system. For instance, longer sonication times or more powerful ultrasound sources may be necessary to achieve the desired results in solutions with higher viscosity [17,25,31]. In that sense, the use of a horn might be for example a better option, compared to an ultrasonic bath [31]. Nevertheless, despite the potential of US processing of high viscosity products, there is only a limited number of investigations related to design and operational aspects of sonochemical applications in viscous solutions [17,36].

In our previous study [41], we investigated the effectiveness of ultrasound in viscous systems using a specific experimental setup. It was observed that the efficiency of energy utilization and the distribution of cavitationally active zones are non-linear and strongly influenced by the viscosity of the solutions, as well as by geometric parameters, such as the immersion depth of the horn which plays a crucial role in defining the irradiating surface submerged in the liquid. Building upon our previous work, the current paper presents a more comprehensive analysis focusing on two main geometric parameters: the shape/diameter of the horn tip, which modifies the available irradiating area, and the size/-diameter of the vessel, which affects the interactions between the horn and the reactor walls and potentially affects the acoustic activity in the system. Additionally, two different US devices with varying power rating were utilized. The combination of these parameters was studied in connection with the viscosity of the solutions, aiming to enhance the understanding of the relationship between ultrasound and viscosity, and to highlight the importance of thoroughly characterizing a sonochemical setup. This approach offers valuable insights for the design of ultrasound-assisted polymer processes, closely reassembling the viscosity range encountered during the initial phases of polymerization reaction.

Specifically, solutions with viscosities ranging from 1 to ≈3000 mPas were prepared and subjected to sonication. The choice of this viscosity range was not arbitrary, as it encompasses the viscosity values of reactants commonly used in the production of polyurethanes with increasing chain length diols [10]. For instance, the initial viscosity remains below 50 mPas when using monoethyelene or diethylene glycol. On the contrary, when using higher chain length diols like polyethylene glycol with molecular weight of 200 or 400, the viscosity is in the range of 50 and 100 mPas respectively. This approach allowed the investigation of the influence of viscosity on the calorimetric energy input, the distribution of cavitational active zones using SCL, and the formation of bubble clusters by HSC imaging. The experiments were conducted in two lab scale batch reactors using a horn device positioned in two insertion depths inside the vessel. The power rating of the US device was varied from 50 to 200 W, horn tips of different diameters (ranging from 3 to 7 mm) were tested, and vessels with different capacities were used. Furthermore, an unconventional horn design consisting of an inverted cone structure was tested, aiming to produce a more homogeneously distributed cavitation zone in the reactor [42].

2. Experimental section

2.1. Materials

Water and polyethylene glycol (PEG) of varying molecular weight, were thoroughly mixed in the same mass fractions (40 wt%) for the preparation of solutions with increasing viscosity. PEG with number average molecular weight of 400 g/mol (maximum water content 0.5%) was purchased from Sigma Aldrich. PEG with molecular weight 2000, 4000, 8000, 20000 and 35000 g/mol (purity >99.5%) were provided by Clariant. The glycols will be named “PEG400”, “PEG2000”, “PEG4000”, “PEG8000”, “PEG20000” and “PEG35000” for simplicity hereafter. For the sonochemiluminescence (SCL) method, luminol with purity >96.5% was purchased from Sigma Aldrich and sodium hydroxide (micro pearls for analysis) from Acros Organics. All chemicals were used as received. MilliQ water (18.2 MΩcm) was used for the preparation of the solutions.

2.2. Properties measurement

The physicochemical properties of the solutions were obtained experimentally at different temperatures (between 23 and 90°C). The detailed protocols for all measurements can be found in our previous work [41]. Briefly, the measured properties included:

- The viscosity (μ) and density (ρ) of the samples, which were obtained simultaneously using an Anton Paar Lovis 2000 ME/DMA 4500 viscodensity meter.
- The isobaric specific heat values (c_p), determined using a DSC-Q2000 from TA Instruments.
- The speed of sound (c) measurements were performed using a ResoScan acoustic interferometer from TF-instruments. A detailed description of the method can be found in the study by Pfeiffer et al. [43].
- Surface tension (σ) measurements were conducted using a Krüss K100C tensiometer (Wilhelmy plate method).

Additionally, the pH of the solutions used for the SCL experiments was determined using a calibrated pH combination electrode (sphere membrane, A-glass). The mixtures were prepared in triplicate and the pH measurements were taken after 1h of homogenization at room temperature.

2.3. Experimental setups

Various experimental setups were created by combining the following elements:

- Two glass reactors filled with approximately 130 (reactor A) or 60 ml (reactor B) of solution;
- Two US processors (Hielscher Ultrasonics) operating at similar frequency (30 and 24 kHz), rated power of 50 W (UP50H) and 200 W (UP200S). All experiments were performed at 100% amplitude;
- Three horn tips of common cylindrical shape (MS3, MS7 and S7), and a special cone-shape horn tip (compatible only with the 200 W device), all from Hielscher Ultrasonics. The material of construction of all the tips was titanium.

In all experiments the ultrasonic horn was centrally inserted from the top of the reactor and placed in the desired insertion depth using a translation stage. A schematic overview of the different setups, can be seen in Fig. 1. The dimensions of the vessels are presented in Table 1.

The elements presented in Fig. 1 were combined to create seven different setups, for which details and specifications can be found in Table 2.

2.4. Calorimetric efficiency measurements

The electrical power input to the ultrasonic source was related to the power transferred to the medium with calorimetric experiments using multiple temperature probes similar to our previous work [41]. Using the temperature rise (dT/dt), the mass of the medium (m_{medium}) and the specific heat constant (c_P), the calorimetric power (P_{cal}) was calculated (Eq. 1) and correlated to the electrical power (P_{el}) and calorimetric efficiency (η_{cal}) using Eq. 2. The power density was calculated using Eq. 3.

$$P_{cal} = m_{medium}.c_p.\frac{dT}{dt} \quad \text{(Eq. 1)}$$

$$\eta_{cal} = \frac{P_{cal}}{P_{el}} \quad \text{(Eq. 2)}$$

$$Power\ density = \frac{P_{el}\ or\ P_{cal}}{m_{medium}} \quad \text{(Eq. 3)}$$

2.5. Sonochemiluminescence (SCL) technique

The sonochemiluminescence (SCL) method was used to visualize the

Table 1
Dimensions of the reactors used for the experiments.

Reactor	Diameter - D_R (mm)	Height - H_R (mm)	Bottom plate thickness (mm)	Jacket[1] thickness (mm)
A	52.6	80.9	7.3	16.7
B	35.0	108.3	9.0	13.0

Note[1]: Cooling water circulated in the jacket via a thermostatic bath (Lauda Eco Silver RE630) to achieve the desired temperature.

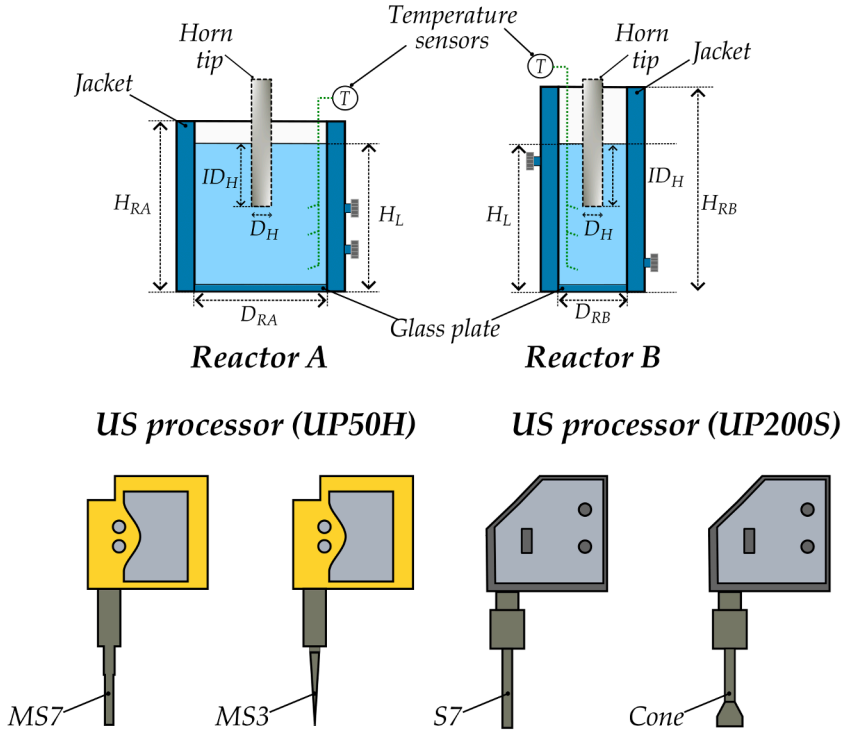

Fig. 1. Schematic representation of the experimental setups, using reactor A and B and two US processors (50 and 200 W power rating). Key: $D_{R,i}$: reactor diameter of reactor i, D_H: horn diameter, $H_{R,i}$: reactor height of reactor i, H_L: liquid height, ID_H: horn insertion depth.

Table 2
Overview of technical specifications and combinations of the ultrasound sources used.

Reactor	Working capacity (ml)	Device	Operating frequency (kHz)	Maximum power (W)	Tip name	Tip diameter - D_H (mm)	Maximum amplitude[3] (μm)
A	130	UP50H	30	50	MS3	3	180
					MS7[1]	7	125
		UP200S	24	200	S7	7	175
					Cone[2]	40	12
B	60	UP50H	30	50	MS3	3	180
					MS7	7	125
		UP200S	24	200	S7	7	175

Note[1]: This setup was used in [41] and is included herein for comparative purposes.
Note[2]: The name "Cone" is used for simplicity, it refers to a sonotrode of increased diameter along its length.
Note[3]: As reported by the manufacturer [44].

spatial distribution of cavitation in the reactors. Briefly, when aqueous solutions of luminol and sodium hydroxide (NaOH) are sonicated, the luminol reacts with sonochemically generated hydroxyl radicals. Upon relaxation, the product of this reaction (3-amino phthalate) emits blue light [2,12], that can be detected and captured using a digital camera. The precise reaction mechanism is complex and still not completely understood. A suggested reaction mechanism [45] can be found in section A1 (Supporting information). From Figure S1, a dependency of emitted light intensity and the solution pH is evident.

For the imaging of PEG-water mixtures, SCL-active solutions were prepared, which consisted of 0.2 wt% luminol and 0.4 wt% NaOH. To maintain a consistent ratio of luminol and NaOH (relative to water), in the water sample the concentrations were increased to 0.33% and 0.72%, respectively. The SCL-active mixtures were sonicated and images were captured inside a completely light insulated box using a Nikon Z6 II digital camera, with a NIKKOR optical lens (Z MC 50mm f/2.8). The exposure time was 15 seconds, the focal ratio was 3.5 and the ISO setting was 25600. The obtained images were processed and analysed to enable semi-quantitative analysis [41].

2.6. High speed imaging

To visually observe the formation of bubble clusters at a macroscopic scale a high-speed camera (Fastcam Mini UX100 Photron) was used, connected to a Tokina optical lens (AT-X M100 f/2.8 PRO D Macro) and controlled using the Photron Fastcam viewer (PFV4) software. Images were recorded a using a frame rate of 250 fps and a shutter speed of 1/250 seconds. A LED-light, connected to a DC power source, was placed behind the reactor to ensure proper lighting.

3. Results and discussion

3.1. Properties of prepared solutions

An overview of the different characteristic properties of the custom-made mixtures can be found in Fig. 2.

A significant increase in viscosity of up to three orders of magnitude was achieved, with the liquid viscosity (μ) varying approximately from 1 mPas for water to 3000 mPas for the 40 wt% PEG35000 solution (Fig. 2a). The temperature dependency of the samples viscosity is presented in Figure S2. The density (ρ) of the PEG-water mixtures remained rather independent of the molecular weight of PEG employed (Fig. 2b). Only a small difference between the pure water (0.998 g/cm^3) and the PEG-water mixtures (average of ≈1.069 g/cm^3) was observed. Subsequently, the specific heat capacities (c_p) of the solutions were obtained (Fig. 2d). For reference, the heat capacity values of the PEGs that are solid at room temperature (PEG2000 and higher) were also measured (Fig. 2c). A first observation is related to the melting temperature range of the solids, which increased for higher molecular weight (MW) PEGs. The presence of overlapping regions among the various polymers, indicates that possibly the PEG powders potentially consist of mixtures containing various MW polyols rather than being solely composed of a single MW polyol [46]. The c_p values for the PEG-water mixtures (Fig. 2d) show a decreasing trend as the MW of PEG increases. This indicates that mixtures containing longer PEG molecules require less heat to increase in temperature. One possible explanation for this observation is the difference in internal energy, which is influenced by intermolecular forces such as hydrogen bonding between water and PEG. The addition of short-chain PEG molecules leads to a higher number of hydrogen bonded interactions with the water molecules, resulting in stronger intermolecular connections compared to adding a smaller amount of longer-chain PEG molecules. Therefore, the overall mobility of the system may be reduced in the case of low molecular weight PEG molecules, requiring a higher input of heat to achieve a sufficient rise in molecular kinetic energy and subsequent temperature increase [46,47]. The measured sound velocity of the various mixtures can be seen in Fig. 2e. Two main observations can be made; Firstly, the addition of PEG to the mixture significantly changes the speed of sound. This change can be attributed to modifications in compressibility resulting from the alteration of intermolecular forces within the PEG-water hydrogen bonding network [48]. Secondly, it is observed that the molecular weight of the PEG does not have an important impact on the speed of sound value. Finally, the addition of PEG into water causes a substantial reduction in surface tension (σ) values (Fig. 2f). This phenomenon has been observed by other researchers [49]. The decrease in surface tension can be attributed to the alteration in intermolecular bonding between water molecules, as a result of inclusion of PEG-water interactions. When comparing PEGs with different molecular weights, no clear trend was remarked, with the values fluctuating in the range of 50-57 mN/m.

3.2. Impact of viscosity increase on calorimetric power

The results of the measured electrical and calorimetric power input for the various setups are presented in Fig. 3 for 35 mm insertion depth of the horn. Insertion depth of 25 mm was also evaluated and these results are available in Figure S3. As described earlier, ultrasonic horns are typically designed to provide a designated tip (set) amplitude, and the devices regulate their electrical input power to achieve this desired motion. In the experimental study presented herein, the devices were set to produce the highest achievable tip amplitude (100% setting). Consequently, the energy input to the transducer is automatically adjusted to achieve the targeted tip displacement.

A first observation when comparing the two reactors is that despite the significant difference in vessel volume, the calorimetric power input for reactor A and B remained relatively similar [11]. The same was noted for the 25 mm insertion depth (Figure S3). This suggests that the calorimetric power density of the smaller reactor B is at least two times higher than that of the larger reactor A [11,50], which was confirmed

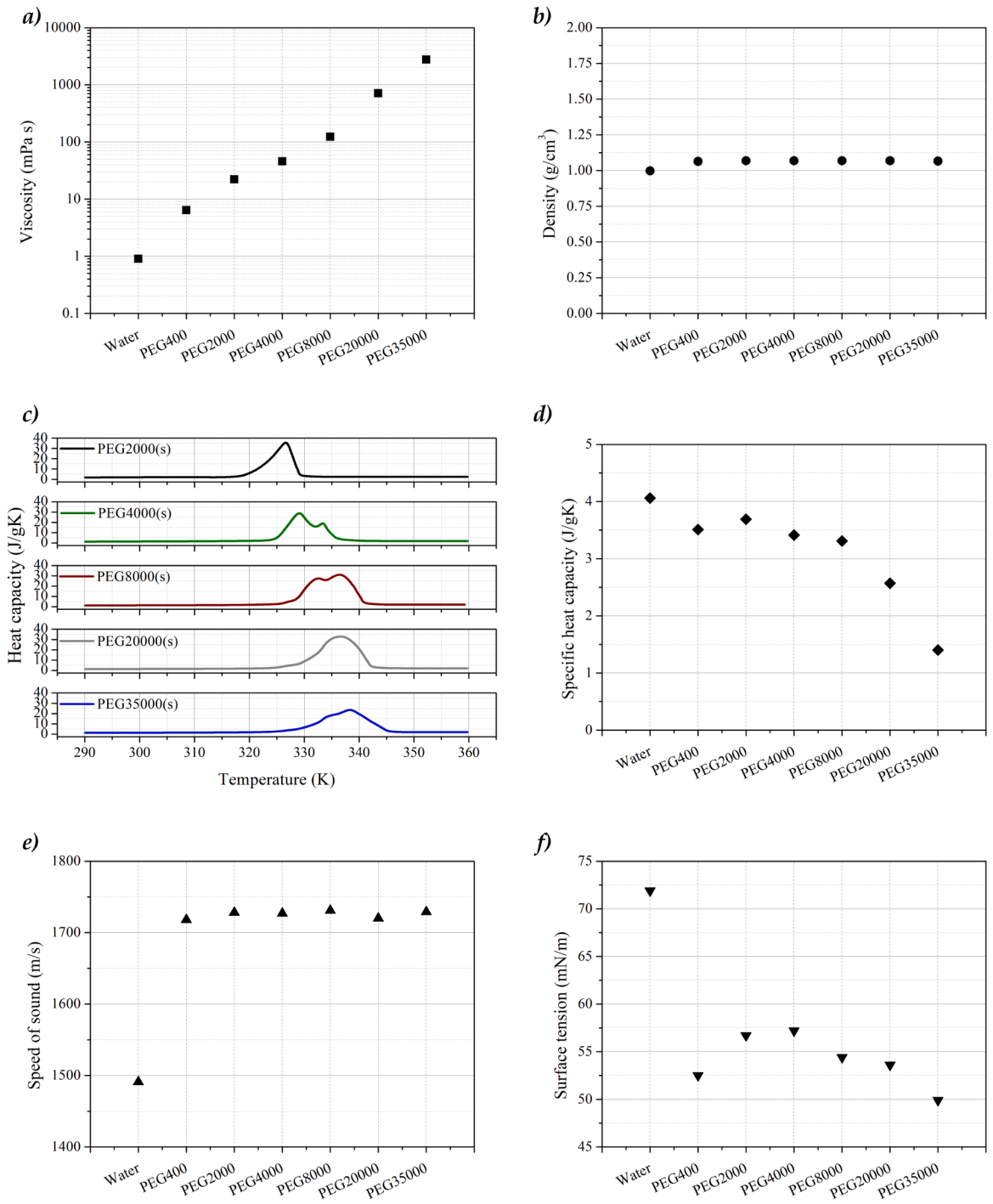

Fig. 2. Properties of prepared water-PEG solutions at 23°C: a) Viscosity b) Density d) Specific heat capacity values e) Speed of sound and f) Surface tension. Note: for simplicity, only the name of the polyol used for the 40 wt% solution is noted on the x-axis. Heat capacity values of solid PEGs against temperature are plotted in c) for reference, data based on the third heating cycle (consecutive heating-cooling cycles repeated twice).

even for the most viscous solutions tested (Figure S4, Figure S5). These results highlight the potential of ultrasound in small scale reactors, particularly in the context of US-assisted microreactors [25]. Nevertheless, the use of microreactors, despite their promising applications, may present certain challenges in high viscosity applications. The occurrence of significant pressure drops and the potential for clogging can pose serious disadvantages [51].

A notable finding is the relationship between viscosity and the maximum electrical power consumption of each setup, as seen in Fig. 3. Across all systems examined, it was observed that the electrical power exhibited an increasing trend, followed by a sharp decrease, accompanied by discontinuous operation [41]. As mentioned before, the US devices used herein are designed to operate at a set amplitude, therefore they modify their electrical power consumption accordingly. When the required electrical power input exceeds the safe power rating of the device, it switches to pulsing-mode to protect its internal structures [44]. This behavior was observed in the sample with the highest viscosity (≈2770 mPas) for the UP50H-MS3 setup (Fig. 3, *i*), in the sample with ≈123.2 mPas viscosity for the UP50H-MS7 setup (Fig. 3, *ii*), and in the sample with the highest viscosity for the UP200S-S7 setup (Fig. 3,

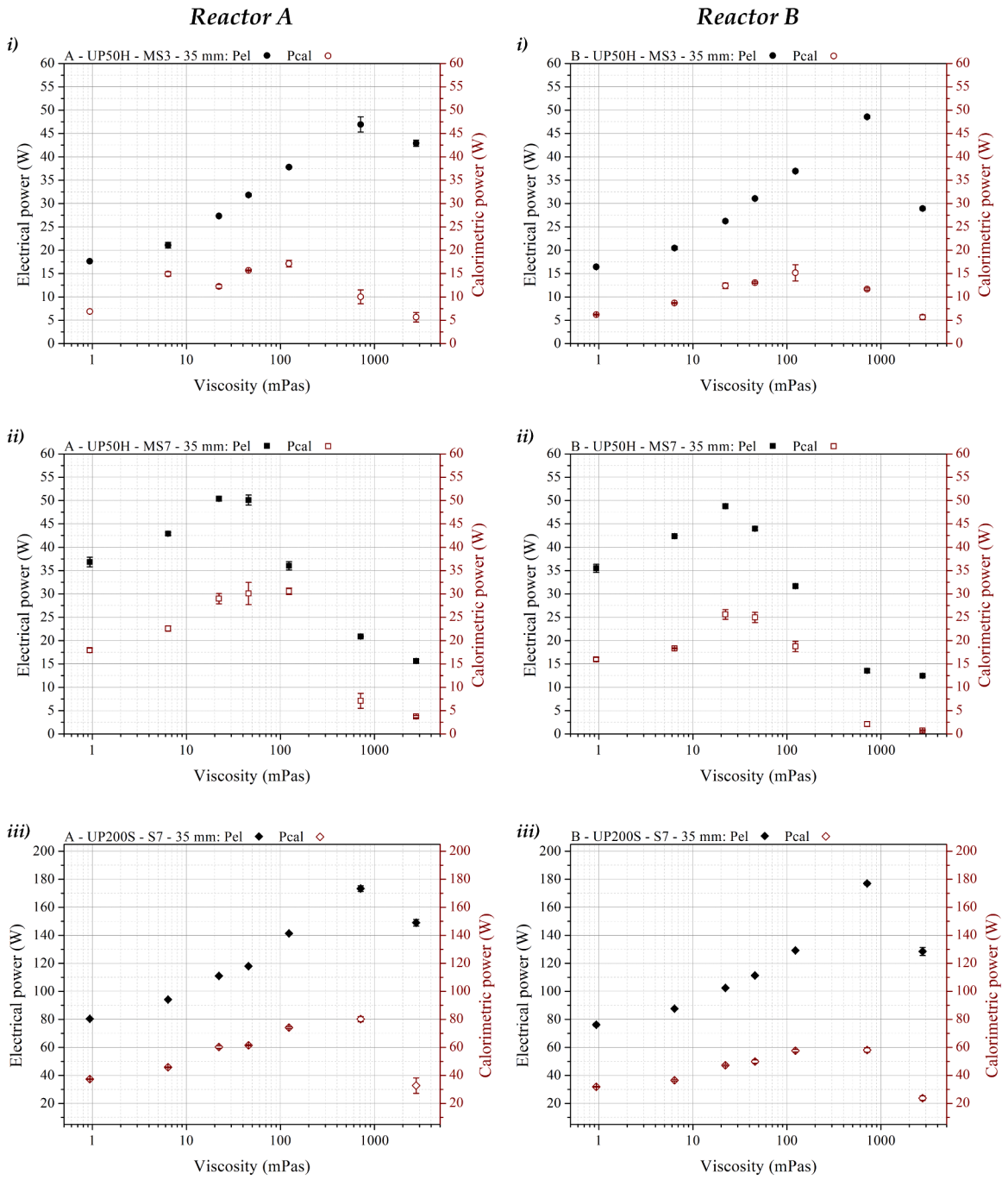

Fig. 3. Measured electrical and calorimetric power for sonication using the UP50H and the UP200S device, liquid height of 60 mm, set amplitude of 100%, and horn insertion depth of 35 mm. Results for reactor A (≈130 ml, left) and reactor B (≈60 ml, right) - MS3 i), MS7 ii), S7 iii). Standard deviation values based on three replicates are included in the graphs.

iii), which was similar to the MS3 tip. Interestingly, the drop in electrical power input was correlated with poor heat dissipation in the solution resulting in large temperature gradients [41]. Examples from online temperature recordings are presented in Figure S6. The continuous operation of the system showed an extended duration in two cases: when the smaller tip diameter (MS3) was used (comparing the setups using the UP50H device) and when the more powerful device was used (comparing UP200S-S7 to UP50H-MS7). This indicates that the MS3 tip requires less power to maintain the set amplitude, potentially due to reduced drag on the sonotrode tip caused by its smaller diameter or by the smaller weight of the horn tip that needs to be displaced within the bulk. For the setups with larger diameter tips, the crucial factor is the rated power of the device, with the UP200S device being rated four times more powerful than the UP50H [44].

When considering the setups using the UP50H device (Fig. 3 *i* and *ii*) for both reactors, it was observed that the use of the smaller diameter tip (MS3) resulted in lower electrical and calorimetrical power compared to the MS7 tip for viscosities up to ≈50 mPas. At viscosity of 123.2 mPas (40 wt% PEG8000 solution), the electrical power (P_{el}) consumption of the two systems was found to be similar (37.8 W for the MS3 and 36 W for the MS7). However, for this solution the MS7 demonstrated higher efficiency (84.9% for the MS7 and 45.3% for the MS3) as shown in Figure S7, attributed to the discontinuous operation of the device which led to lower electrical power consumption. It is worth noting that the

efficiency of both setups decreased considerably for the two highest viscosity solutions (≈ 1000 and 3000 mPas), with efficiency below 20% for the MS3 and below 34% for the MS7 (Figure S7). When comparing the results for the UP200S-S7 and UP50H-MS7 setups (Fig. 3 *ii* and *iii*), it is evident that both the electrical (P_{el}) and the calorimetric (P_{cal}) power inputs were higher for the former, due to the higher nominal sonotrode amplitude of the UP200S-S7 (Table 2). A larger amplitude requires more electrical power to operate and results in increased heat generation. As previously mentioned, the efficiency of the MS7 tip showed an increasing trend up to approximately 100 mPas, followed by a sharp decrease for the highest viscosities. In contrast, as presented in Figure S7 *iii*), the efficiency of the S7 tip remained almost constant (approximately 50%) for all the solutions sonicated, except the highest viscosity solution (efficiency of 22% for the 40 wt% PEG35000). In both reactor geometries, the comparison between the UP200S-S7 with the UP50H-MS7 setup, showed that using the former configuration postponed the decrease in electrical and calorimetric power until the highest viscosity range, similar to the observations made with the MS3 tip. It is interesting to note that when water was sonicated, the efficiency remained relatively unaffected across the different reactor-sonotrode configurations (40-50%). For a complete overview of the efficiency and the power density of the setups, reference is made to the Supporting information (Figures S4-S5, Figures S7-S8).

Overall, in order to achieve successful sonochemical assistance of a process, an efficient energy input to the reactor is desirable. Therefore, the choice of the appropriate transducer becomes a crucial design

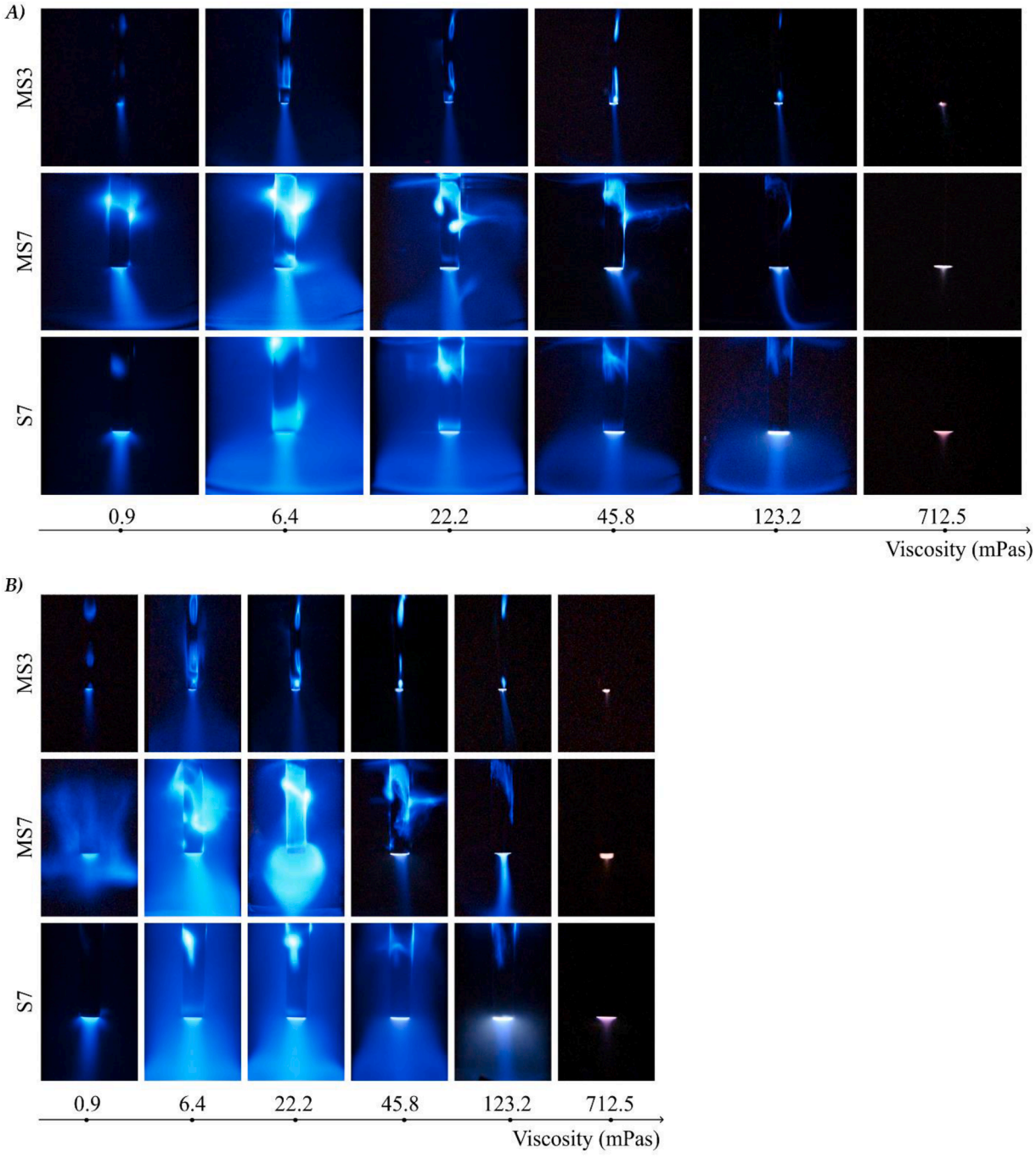

Fig. 4. SCL images for increasing viscosity solutions in reactor A (top) and B (bottom), liquid level of 60 mm, set amplitude of 100% at horn insertion depth of 35 mm: UP50H (50 W) when MS3 and MS7 horn tips were used (first two rows) and UP200S (200 W) when S7 horn tip was used (last row).

parameter for optimizing applications, particularly in viscous solutions. It should be emphasized here that the power rating of an ultrasonic device should not be mistaken as the ultrasonic power input to the reactor. As evident from the calorimetric data presented herein, only part of the electrical power is being converted to heat. Additionally, each device has distinct design characteristics that result in diverse responses under extreme conditions. For instance, the point at which non-continuous operation or system limitations are reached may differ across devices. Nevertheless, similar observations are anticipated when using ultrasonic horn systems from different manufacturers.

The aforementioned observations have also practical potential. In the context of applying ultrasound to polymer synthesis, for instance, varying power-rated horns might be required based on the polymerization stage. During initiation, a lower-rated system could be adequate for brief pulsations. If additional assistance is needed as the reaction progresses, higher-rated power devices could be activated. This concept of utilizing multiple systems could be applicable in a reactive extrusion process, where lower-power US devices are employed in the initial extruder barrels and more potent ones are positioned along the extruder's length.

3.3. Sonochemiluminescence (SCL) and luminol intensity results

The sonochemiluminescence (SCL) method was employed for the visualization of cavitationally active zones in both reactors. An overview of the obtained images for 35 mm horn insertion depth is presented in Fig. 4 and for 25 mm can be found in Figure S9. The 40 wt% PEG35000 solutions were not included in the SCL analysis due to poor dissolution of the luminol in the bulk.

It should be noted that the SCL images for water and for all setups, have been included in the overviews for reference. The presence of the polyol in the solutions alters important physicochemical parameters of the solutions compared to water (e.g. the surface tension and speed of sound, Fig. 2) making a proper comparison not possible [41]. Moreover, introducing an organic compound, such as polyethylene glycol, could potentially bring alterations in the radical generation and consumption within the system. On the contrary, for the PEG-water mixtures the properties are marginally affected by the molecular weight of the PEG, which indicates the decrease in light emission between the different PEG-water SCL mixtures can be mainly attributed to the increase in viscosity. Another important parameter that was examined to verify the difference between water and PEG-water solution, was the pH of the SCL-active mixtures. The results are presented in Figure S10 and show that the addition of PEG alters the pH of the SCL mixtures, with the pH of the PEG based solutions being approximately 4% higher (average of 13.5 compared to 12.9). As highlighted in section 2.5, there is a pH dependency on the intensity of sonochemiluminescence [45]. Additionally, the pH seems relatively insensitive to the molecular weight of the polyol used and remained almost unchanged for the PEG-water solutions.

When sonicating the solutions with the MS3 tip connected to the UP50H device (Fig. 4A, B), two main observations can be made; Firstly, the intensity of the zones showed an overall decreasing trend for PEG-water solutions of increasing viscosity, confirming findings of our previous work [41]. Secondly, multiple zones were found along the horn: one zone located directly at the tip of the horn and two zones along the horn shaft for viscosities up to ≈50 mPas. For viscosity of approximately 100 mPas two zones remain (the third one decreased significantly) and for the highest viscosity tested (approximately 1000 mPas) light only at the tip of the horn remained visible. The appearance of multiple zones along the shaft of the horn is associated with the radial movement of the horn, which expands and contracts during sonication of a solution. This phenomenon was explained by other researchers as the "flow of acoustic energy through the lateral boundaries of the transducer" [52]. The decrease or disappearance of the radial cavitation zones, may be conjectured to partially explain the reduction of calorimetric power for viscosities above 100 mPas (Fig. 3 *i*). The findings were similar for both reactors tested (Fig. 4A and B, MS3).

The main observations related to the MS7 (UP50H) and S7 (UP200S) setups could be summarized in the following points: two cavitation zones can be seen, one directly under the horn tip and one covering the horn shaft. For the most viscous sample (40 wt% PEG20000), the cavitation zone covering the horn wall completely disappeared, even when the more powerful UP200S horn was used. Furthermore, the use of the UP200S does not always increase the SCL light intensity and overall, the images appear less bright than those using MS7 (UP50H). For example, in reactor A (compare second and third lines on Fig. 4A), the zone around the horn shaft decreased more significantly with the solution viscosity when the S7 (UP200S) was used. However, the calorimetry results obtained for the same setups (Fig. 3, left column, *ii* and *iii*) demonstrate globally higher P_{cal} for the UP200S than for the UP50H. Therefore, this suggests that larger calorimetric power is not necessarily concomitant with the formation of larger/brighter SCL zones. This may be explained by the presence of a more densely packed, strongly oscillating bubble cloud under the transducer in the case of UP200S, that consumes a larger amount of acoustic energy, yielding a larger P_{cal}, but strongly attenuating the sound wave, limiting its transmission to secondary zones of the reactor [19,38,50].

Focusing on the results of reactor B sonicated by the UP50H horn with a MS7 tip, resonance-like phenomena were observed (Fig. 4B, MS7). For pure water, a large blue cloud of SCL emissions, covering the whole reactor was noticed. However, the calorimetry results do not indicate an increase in dissipated power compared to reactor A (compare red points on the *ii*) graphs in Fig. 3). This suggests again that the structure and brightness of luminol SCL maps is not trivially correlated to the power dissipated in the liquid. When the horn insertion depth is lowered to 25 mm (Figure S9) or when a different reactor geometry is chosen (Fig. 4A, MS7), the large blue cloud decreased considerably and was limited to a zone below the tip and around the horn shaft. Remarkably, for the same setup and for viscosity of 22.2 mPas (Fig. 4B, MS7, third image), a "bulbous" or "elongated bubbly" shaped zone of light emission below the horn tip was captured similar to what was reported for concentrated sulfuric acid [53] and glycerine solutions [32], respectively. This bulbous shaped zone is not visible in reactor A (Fig. 4A, MS7, third image). The above results indicate that a careful choice of reactor geometry is of paramount importance in developing sonochemical systems [11,19].

A general noteworthy observation related to the multiple cavitation zones along the submerged horn walls is the asymmetrical distribution of SCL light along the two sides of the horn walls. Cavitation activity that is not centered has been observed in other studies as well, commonly at lower tip amplitude [34]. This could be considered a result of the very dynamic and sensitive nature of acoustic cavitation [12]. Furthermore, the SCL images were semi-quantitatively analyzed by averaging the luminance of each image, which provides a global brightness indicator following the intuitive visual perception. For each configuration, these quantitative results were plotted in function of the solution viscosity. These plots can be found in the Supporting Information (Figure S11 and Figure S12).

Examining the calorimetric power and SCL results presented earlier, it becomes evident that the observations obtained do not always align, highlighting a fundamental challenge in characterizing sonochemical reactors. Each method has its own advantages and limitations, and there is no universal approach that can be applied to quantify the sonochemical performance of any reactor. For instance, the calorimetric method provides integral information on energy dissipation and cannot be directly correlated to the extent of acoustic cavitation. In contrast, the SCL method provides insights into the size of cavitation zones, and is a sensitive technique to the composition of the sonicated solution. Therefore, combining multiple characterization techniques is preferred, as this approach can provide valuable insights during the process design phase.

Lastly, the SCL results have direct relevance in polymer synthesis. As the reaction progresses and the molecular weight and viscosity of the products increase, the number of cavitation zones is expected to decrease significantly. If the synthesis mechanism relies on radicals produced sonochemically, the SCL results can provide crucial insights for the implementation of sonication strategies.

3.4. High speed imaging results

In order to get more insights in the SCL results (Fig. 4), High speed camera (HSC) imaging of the UP50H device with the MS7 tip was performed. The results presented in Fig. 5, showed for most cases good correspondence with the SCL images: for water, bubble clusters are visible both at the tip and the shaft of the horn. For the 40 wt% PEG400 (or 6.4 mPas) mixture, the second cavitation zone around the horn shaft is more pronounced in both reactors. At the next viscosity step (22.2 mPas) for reactor B, the "elongated bubbly structures" below the horn tip that were observed with SCL (Fig. 4B, MS7, third image), were confirmed. Similar structures were noticed for glycerine, behaving like elastic shells consisting of a bubble-shaped core followed by a bubbly trail [32].

When comparing SCL and HSC images, it must be recalled that the latter are snapped over a 4 ms exposure time, whereas the former are integrated over 15 s exposure. Thus, it can be expected that the bubble structures are almost frozen by HSC but may move and deform noticeably during SCL exposure. The resulting SCL images may, therefore, integrate the successive locations of a given structure observed in HSC images. This can be exemplified for vessel A with 6.4 mPas mixture: the bended filamentary structure visible in the HSC image (Fig. 5, first row, second image), originating from the top of transducer lateral area, probably moves slowly and results after 15 s exposure in the two-lobes structure with very bright SCL light, visible in Fig. 3A, second row, second image. The same kind of mechanism may be conceptualized for the 22.2 mPas images: HSC reveals a small cluster attached to the transducer lateral area, whereas its corresponding SCL map displays an enlarged spot at the same location. The second one, visible slightly below on the right is not visible on HSC probably because it was hidden by the transducer shadow.

Finally, it is worth noting that although a distinct bright zone was only visible below the sonotrode tip with SCL for the 712.5 mPas sample (Fig. 4, second row, last image), the HSC images revealed additional structures reassembling a droplet hanging from the transducer. These structures appeared darker near the symmetry axis and were more elongated in the case of reactor A. This "inverted mushroom" shape was also observed in the case of glycerine when the maximum tip amplitude was applied [32].

3.5. Mapping reactor A using a special shape horn tip

In the last section, a different sonotrode design is examined, called the "cone" tip which can operate connected to the UP200S device and was tested only in reactor A. Anticipated advantages associated with the unique design of this tip were expected, as it allows for a more dispersed distribution of ultrasonic energy within the reactor, thereby reducing cavitation shielding and minimizing sonotrode damage [42]. The electrical and calorimetric measured power for horn insertion depth of 35 mm are presented in Fig. 6, the results for 25 mm being deferred to Figure S13.

The electrical power consumption does not exhibit a clear trend and demonstrates a more scattered pattern, contrary to the results for the cylindrical tip designs shown in Fig. 3. Globally, the electrical and

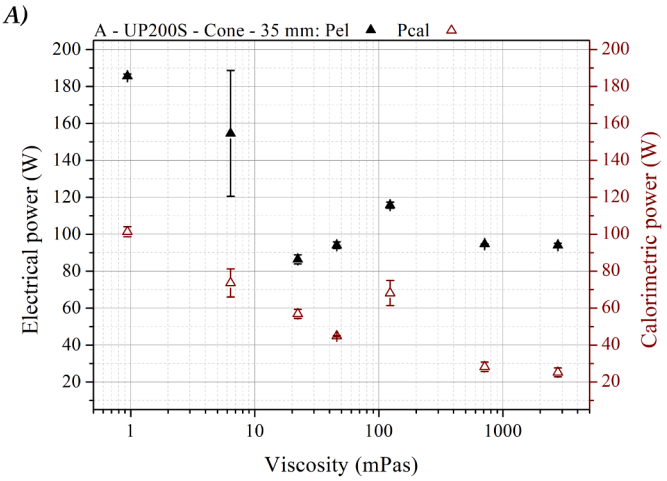

Fig. 6. Measured electrical and calorimetric power for sonication using the UP200S device, liquid height of 60 mm, set amplitude of 100%, and horn insertion depth of 35 mm. Results for reactor A using the cone shape tip. Standard deviation values based on three replicates are included in the graphs.

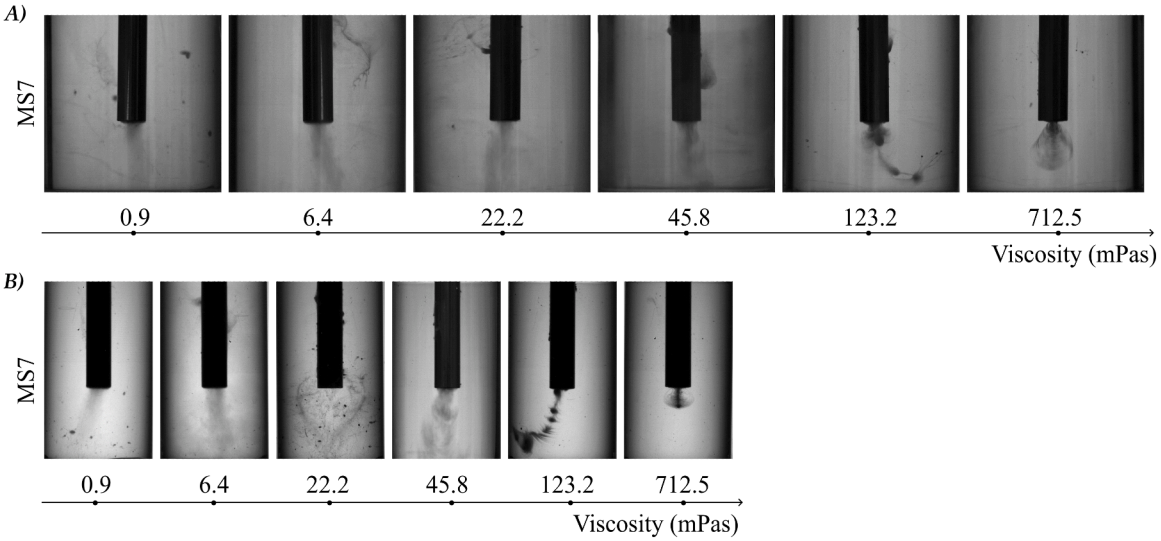

Fig. 5. HSC images for increasing viscosity solutions in reactor A (top) and B (bottom), liquid level of 60 mm, set amplitude of 100% at horn insertion depth of 35 mm: UP50H (50 W) and MS7 horn tips were used.

calorimetric power follow the same trends with the exception of a single point, being the 22.2 mPas solution. For this viscosity, a precipitous decrease of the P_{el} is noticed compared to the 6.4 mPas. While the exact reason for this deviation remains unclear, it might be partly explained by variations in the transducer impedance resulting from the creation of cavitating standing wave regions that may modify the electrical power consumption [19,50]. The presence of standing wave zones is discussed in the SCL analysis that follows (Fig. 7). Specifically, it seems that from 6.4 to 22.2 mPas a qualitative transition occurs in the pressure field, characterized by the appearance of two distinct cavitation zones, spatially separated with a dark zone in between. These zones could potentially influence the movement of the sonotrode. Alternatively, the limited space between the cone lateral side and the reactor wall (≈ 6 mm), could obstruct harmonic sonotrode movement due to viscous hydrodynamic boundary layers or increased drag form. The power density and efficiency were also estimated for the cone-sonotrode setup. Excluding the viscosity points of 22.2 and 123.2 mPas, a reduction in efficiency was noted as the mixtures viscosity increased. An overview of the results is available in Figure S14.

Similar to the conventional horn-shaped configurations, the SCL technique was applied for the cone setup as well. An overview of the images captured at a depth of 35 mm is presented in Fig. 7, while those obtained at a depth of 25 mm can be found in Figure S15.

Several interesting observations can be made based on the SCL results: Firstly, the intensity of the light emitted for water is more intense compared to the PEG-water solutions in contrast to the cylindrical tip configurations. The estimated power density showed a maximum for water as well (Figure S14). Secondly, for the solutions with viscosity ranging from 6.4 to 123.2 mPas, multiple cavitation zones are noticed. One zone was located around the shaft of the cone sonotrode, and the second zone was observed below the tip. Specifically, for a viscosity of 6.4 mPas, the former zone was located around the cylindrical part of the cone, while for the viscosities of 22.2 and 45.8 mPas, this zone was noticed at the contraction of the shaft. Moreover the cavitation zone below the tip did not form directly under the tip but at a distance of $\lambda/2$ (counted from the cone surface to the bottom of the reactor), with λ being the wavelength. This observation suggests the presence of a standing wave pattern below the cone sonotrode [50]. Interestingly, in the case of a viscosity of 123.2 mPas, the formation of a standing wave was not observed, despite the fact that the solution had the same wavelength as the other cases. This can be attributed to the higher viscosity, which led to increased energy attenuation. As a result, a stronger travelling wave was formed instead of a standing wave [35,54]. Thirdly, an interesting transition in the luminol structure shape under the sonotrode can be observed: in the case of water and the 123.2 mPas viscosity sample, a “cone-like bubble” structure is observed. It is noteworthy that for both viscosity points, the power density results are the highest recorded (Figure S14, second row, first image). This type of irradiating structures, known as cone-like bubble structure (CBS), have been previously observed during sonoluminescence experiments when sonication was applied to water using large diameter sonotrodes (20-120 mm) [55]. For viscosity values ranging from 6.4 to 45.8 mPas, an extended round structure is observed below the irradiating surface. Finally, no zone was visible for viscosity of 712.5 mPas. The semi-quantitative global brightness analysis results are presented in Figure S16 for both insertion depths of 35 and 25 mm. The findings corroborate the observation that the highest light emissions are observed for water, in contrast to the cylindrical horn tips.

Comparing directly the trends for the cone and the cylindrical S7 tip (for reactor A - UP200S configuration), it becomes evident that for the sonication of solutions with viscosity of 1 to 22.2 mPas the cone sonotrode resulted in increased power density (both electrical and calorimetric), and energetic efficiency compared to the S7 tip (Figures S4, S5, S7, S8 compared to S14). On the contrary, for solutions with viscosity from 45.8 mPas and higher no clear power density and efficiency trends can be remarked and a comparison should be made case by case. Moreover, as mentioned earlier, for the cone configuration it stands out that the SCL light intensity for sonication of water is substantially higher compared to the light intensity of the PEG-water solutions. This is not the case for the S7 sonotrode, for which the opposite trend is observed (Figures S11, S12 compared to S16).

4. Conclusions and future perspectives

In the current work, various increasing viscosity mixtures representing reactants profiles relevant to polymers chemistry were prepared and their physicochemical properties were determined. The viscosity of the solutions covers the range from 1 mPas to approximately 3000 mPas. Additionally, key parameters relevant to the design of an ultrasound-assisted system, such as reactor dimensions, sonotrode power, horn tip diameter, positioning, and shape, were carefully selected and examined. Multiple characterization methods were employed, to highlight the impact of medium viscosity and other design parameters on the sonochemical effects and draw valuable insights for potential applications in polymeric systems.

Several noteworthy findings have emerged from this study, with two key factors influencing the continuous operation of the setups: the diameter of the horn and the power rating of the device. The uninterrupted operation is maintained up to approximately 1000 mPas when utilizing either the more powerful device (rated 200 W) or the lower power device (rated 50 W) with the smaller diameter tip. Moreover, employing a smaller reactor configuration showcases enhanced power density, offering potential benefits for short-duration operations, such as reaction initiation, or continuous flow systems. Additionally, the visualization of cavitation zones using sonochemiluminescence (SCL) imaging reveals the presence of multiple active zones within the reactors. However, it was found that no one-to-one correlation can be established between the brightness and shape of luminol glowing zones and the calorimetric power. Furthermore, resonance-like effects are observed in both water and the 22.2 mPas solution, emphasizing the role of sonotrode-reactor wall distance in optimizing the quantity and intensity of cavitation zones. In general, increase in viscosity of the mixtures leads to a reduction in the number and the intensity of cavitation zones. These findings emphasize the influence of sonotrode and vessel dimensions on

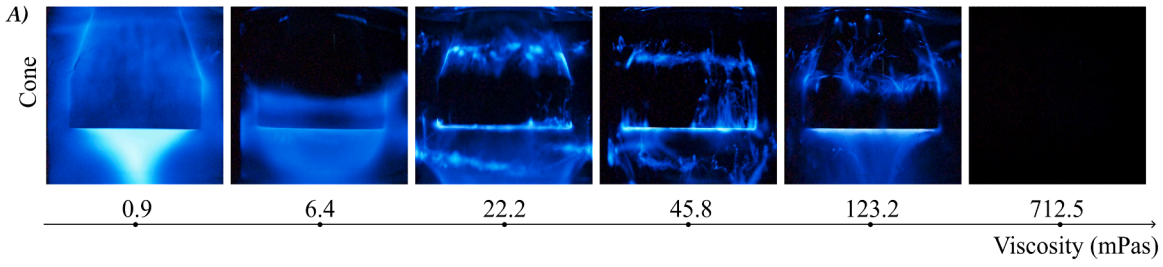

Fig. 7. SCL images for increasing viscosity solutions in reactor A, liquid level of 60 mm, set amplitude of 100% at horn insertion depth of 35 mm: UP200S (200 W) with the cone shape horn was used.

the distribution of these zones along the horn shaft. Such insights are crucial for optimizing and fine-tuning sonochemical processes.

Furthermore, an inverted cone-shaped tip was subjected to characterization, utilizing both calorimetric and SCL analyses. However, the results obtained from these analyses were less conclusive compared to the other configurations studied. It appears that the generation of standing wave patterns becomes more prominent with the cone sonotrode design, as it resembles a plate transducer known to produce both standing and traveling waves. Despite the latter remark, the cone sonotrode setup shows potential if combined with the appropriate configuration. It is important to note that the efficiency of the system decreases significantly when operating with viscosities above approximately 700 mPas.

Our future steps involve integrating the findings from this study with numerical modeling techniques to gain a deeper understanding of the system's performance. This approach will allow us to analyze energy and acoustic pressure distribution as well as fluid flow patterns within the reactor. By combining experimental data with computational simulations, we aim to provide comprehensive insights into the behavior and optimization of the ultrasound-assisted system.

CRediT authorship contribution statement

Ariana Bampouli: Conceptualization, Data curation, Investigation, Methodology, Validation, Visualization, Writing – original draft, Writing – review & editing. **Quinten Goris:** Conceptualization, Data curation, Investigation, Methodology, Validation, Visualization, Writing – original draft, Writing – review & editing. **Mohammed Noorul Hussain:** Data curation, Investigation, Writing – review & editing. **Olivier Louisnard:** Data curation, Investigation, Writing – review & editing. **Georgios D. Stefanidis:** Funding acquisition, Methodology, Supervision, Writing – review & editing. **Tom Van Gerven:** Conceptualization, Funding acquisition, Methodology, Project administration, Resources, Supervision, Writing – review & editing.

Declaration of competing interest

The authors declare that they have no known competing financial interests or personal relationships that could have appeared to influence the work reported in this paper.

Data availability

Data will be made available on request.

Acknowledgments

Funding by the European Union's Horizon research and innovation programmes is gratefully acknowledged by Ariana Bampouli for the SIMPLIFY project (grant agreement No. 820716) and Quinten Goris for the SIMPLI-DEMO project (grant agreement No 101058279). Also VLAIO (Catalisti) is acknowledged for its support of the MMICAS project HBC.2020.2627. The ESS travel grant provided the opportunity for Quinten Goris to perform a fruitful visit to the IMT Mines-Albi institute. We would also like to thank professor Wübbenhorst (department of Physics and Astronomy, KU Leuven) for providing access to the equipment for the speed of sound measurements and Dr. Helge Pfeiffer for the insightful discussions. In addition, the department of Soft Matter, Rheology and Technology of KU Leuven for providing access to the DSC equipment and the department of Chemistry of KU Leuven for providing access to the viscodensity meter and the tensiometer. Finally, our industrial partners at COATEX (Antoine Baldin and Guillaume Michaud) and Clariant for providing the polyols.

Supplementary materials

Supplementary material associated with this article can be found, in the online version, at doi:10.1016/j.cep.2024.109715.

References

[1] G. Cravotto, P. Cintas, Power ultrasound in organic synthesis: Moving cavitational chemistry from academia to innovative and large-scale applications, Chem. Soc. Rev. 35 (2) (2006) 180–196.
[2] D. Rossi, R. Jamshidi, N. Saffari, S. Kuhn, A. Gavriilidis, L. Mazzei, Continuous-Flow Sonocrystallization in Droplet-Based Microfluidics, Cryst. Growth Des. 15 (11) (2015) 5519–5529.
[3] A. Kordylla, S. Koch, F. Tumakaka, G. Schembecker, Towards an optimized crystallization with ultrasound: Effect of solvent properties and ultrasonic process parameters, J. Cryst. Growth 310 (18) (2008) 4177–4184.
[4] M.N. Hussain, S. Baeten, J. Jordens, L. Braeken, T. Van Gerven, Process intensified anti-solvent crystallization of o-aminobenzoic acid via sonication and flow, Chem. Eng. Process. - Process Intensif. 149 (January) (2020) 107823.
[5] J.J. John, S. Kuhn, L. Braeken, T. Van Gerven, Ultrasound assisted liquid–liquid extraction with a novel interval-contact reactor, Chem. Eng. Process. Process Intensif. 113 (2017) 35–41.
[6] R. Jamshidi, D. Rossi, N. Saffari, A. Gavriilidis, L. Mazzei, Investigation of the Effect of Ultrasound Parameters on Continuous Sonocrystallization in a Millifluidic Device, Cryst. Growth Des. 16 (8) (2016) 4607–4619.
[7] T.G. McKenzie, F. Karimi, M. Ashokkumar, G.G. Qiao, Ultrasound and Sonochemistry for Radical Polymerization: Sound Synthesis, Chem. Eur. J. 25 (21) (2019) 5372–5388.
[8] P. Kruus, T.J. Patraboy, Initiation of polymerization with ultrasound in methyl methacrylate, J. Phys. Chem. 89 (15) (Jul. 1985) 3379–3384.
[9] G.J. Price, P.J. West, P.F. Smith, Control of polymer structure using power ultrasound, Ultrason. Sonochem. 1 (1) (1994) 51–57.
[10] G.J. Price, E.J. Lenz, C.W.G. Ansell, The effect of high intensity ultrasound on the synthesis of some polyurethanes, Eur. Polym. J. 38 (8) (2002) 1531–1536.
[11] Y. Son, M. Lim, M. Ashokkumar, J. Khim, Geometric optimization of sonoreactors for the enhancement of sonochemical activity, J. Phys. Chem. C 115 (10) (2011) 4096–4103.
[12] V.S. Sutkar, P.R. Gogate, Design aspects of sonochemical reactors: Techniques for understanding cavitational activity distribution and effect of operating parameters, Chem. Eng. J. 155 (1–2) (2009) 26–36.
[13] J. Jalal, T.S.H. Leong, Microstreaming and its role in applications: A mini-review, Fluids 3 (4) (2018).
[14] S.J. Lighthill, Acoustic streaming, J. Sound Vib. 61 (3) (Dec. 1978) 391–418.
[15] S. Boluriaan, P.J. Morris, Acoustic Streaming: From Rayleigh to Today, Int. J. Aeroacoustics 2 (3) (2003) 255–292.
[16] T. Leong, M. Ashokkumar, S. Kentish, The fundamentals of power ultrasound - A review, Acoust. Aust. 39 (2) (2011) 54–63.
[17] H. Monnier, A.M. Wilhelm, H. Delmas, Influence of ultrasound on mixing on the molecular scale for water and viscous liquids, Ultrason. Sonochem. 6 (1–2) (1999) 67–74.
[18] H. Monnier, A.M. Wilhelm, H. Delmas, The influence of ultrasound on micromixing in a semi-batch reactor, Chem. Eng. Sci. 54 (13–14) (1999) 2953–2961.
[19] Y. Son, Y. No, J. Kim, Geometric and operational optimization of 20-kHz probe-type sonoreactor for enhancing sonochemical activity, Ultrason. Sonochem. 65 (January) (2020) 105065.
[20] P.M. Kanthale, P.R. Gogate, A.B. Pandit, A.M. Wilhelm, Mapping of an ultrasonic horn: Link primary and secondary effects of ultrasound, Ultrason. Sonochem. 10 (6) (2003) 331–335.
[21] D. Sarno, M. Hodnett, L. Wang, B. Zeqiri, An objective comparison of commercially-available cavitation meters, Ultrason. Sonochem. 34 (2017) 354–364.
[22] E. Kim, M. Cui, M. Jang, B. Park, Y. Son, J. Khim, Investigation of sonochemical activities at a frequency of 334 kHz: The effect of geometric parameters of sonoreactor, Ultrason. Sonochem. 21 (4) (2014) 1504–1511.
[23] I. Garcia-Vargas, L. Barthe, P. Tierce, O. Louisnard, Simulations of a full sonoreactor accounting for cavitation, Ultrason. Sonochem. 91 (October) (Dec. 2022) 106226.
[24] K. Fattahi, E. Robert, D.C. Boffito, Numerical and experimental investigation of the cavitation field in horn-type sonochemical reactors, Chem. Eng. Process. Process Intensif. 182 (June) (2022) 109186.
[25] D. Meroni, R. Djellabi, M. Ashokkumar, C.L. Bianchi, D.C. Boffito, Sonoprocessing: From Concepts to Large-Scale Reactors, Chem. Rev. 122 (3) (2022) 3219–3258.
[26] C. Delacour, D.S. Stephens, C. Lutz, R. Mettin, S. Kuhn, Design and Characterization of a Scaled-up Ultrasonic Flow Reactor, Org. Process Res. Dev. 24 (10) (2020) 2085–2093.
[27] M. Ashokkumar, J. Lee, Y. Iida, K. Yasui, T. Kozuka, T. Tuziuti, A. Towata, Spatial distribution of acoustic cavitation bubbles at different ultrasound frequencies, ChemPhysChem 11 (8) (2010) 1680–1684.
[28] C. Agarkoti, P.R. Gogate, Mapping of cavitation intensity in a novel dual-frequency ultrasonic reactor of capacity 10 L, Chem. Eng. Sci. 259 (2022) 117833.
[29] A.S. Mhetre, P.R. Gogate, New design and mapping of sonochemical reactor operating at capacity of 72 L, Chem. Eng. J. 258 (2014) 69–76.

[30] D. Fernandez Rivas, S. Kuhn, Synergy of Microfluidics and Ultrasound: Process Intensification Challenges and Opportunities, Top. Curr. Chem. 374 (5) (2016) 1–30.
[31] J. Berlan, T.J. Mason, Sonochemistry: from research laboratories to industrial plants, Ultrasonics 30 (4) (1992) 203–212.
[32] I. Tzanakis, G.S.B. Lebon, D.G. Eskin, K.A. Pericleous, Characterizing the cavitation development and acoustic spectrum in various liquids, Ultrason. Sonochem. 34 (2017) 651–662.
[33] T. Nowak, C. Cairós, E. Batyrshin, R. Mettin, Acoustic streaming and bubble translation at a cavitating ultrasonic horn, AIP Conf. Proc. 1685 (2015).
[34] L. Yusuf, M.D. Symes, P. Prentice, Characterising the cavitation activity generated by an ultrasonic horn at varying tip-vibration amplitudes, Ultrason. Sonochem. 70 (July 2020) (2021) 105273.
[35] V. Salinas, Y. Vargas, O. Louisnard, L. Gaete, Influence of the liquid viscosity on the formation of bubble structures in a 20 kHz field, Ultrason. Sonochem. 22 (2015) 227–234.
[36] J. Raso, P. Mañas, R. Pagán, F.J. Sala, Influence of different factors on the output power transferred into medium by ultrasound, Ultrason. Sonochem. 5 (4) (1999) 157–162.
[37] Y. Asakura, T. Nishida, T. Matsuoka, S. Koda, Effects of ultrasonic frequency and liquid height on sonochemical efficiency of large-scale sonochemical reactors, Ultrason. Sonochem. 15 (3) (2008) 244–250.
[38] M.M. van Iersel, N.E. Benes, J.T.F. Keurentjes, Importance of acoustic shielding in sonochemistry, Ultrason. Sonochem. 15 (4) (2008) 294–300.
[39] M. Ashokkumar, The characterization of acoustic cavitation bubbles - An overview, Ultrason. Sonochem. 18 (4) (2011) 864–872.
[40] S. Koda, K. Yasuda, Sonochemical Engineering Processes, Elsevier Inc., 2015.
[41] A. Bampouli, Q. Goris, J. Van Olmen, S. Solmaz, M. Noorul Hussain, G. D. Stefanidis, T. Van Gerven, Understanding the ultrasound field of high viscosity mixtures: Experimental and numerical investigation of a lab scale batch reactor, Ultrason. Sonochem. 97 (January) (Jul. 2023) 106444.
[42] Y.C. Wang, M.C. Yao, Realization of cavitation fields based on the acoustic resonance modes in an immersion-type sonochemical reactor, Ultrason. Sonochem. 20 (1) (2013) 565–570.
[43] H. Pfeiffer, G. Klose, K. Heremans, C. Glorieux, Thermotropic phase behaviour of the pseudobinary mixtures of DPPC/C 12E5 and DMPC/C12E5 determined by differential scanning calorimetry and ultrasonic velocimetry, Chem. Phys. Lipids 139 (1) (2006) 54–67.
[44] Hielscher Ultrasonics, "Application of Power Ultrasound using Ultrasonic Horns." [Online]. Available: https://www.hielscher.com/application-of-power-ultrasound-using-ultrasonic-horns.htm. [Accessed: 07-Dec-2022].
[45] H.N. McMurray, B.P. Wilson, Mechanistic and spatial study of ultrasonically induced luminol chemiluminescence, J. Phys. Chem. A 103 (20) (1999) 3955–3962.
[46] J. Chen, S.K. Spear, J.G. Huddleston, R.D. Rogers, Polyethylene glycol and solutions of polyethylene glycol as green reaction media, Green Chem. 7 (2) (2005) 64–82.
[47] J. Wu, S. Chen, Investigation of the hydration of nonfouling material poly(ethylene glycol) by low-field nuclear magnetic resonance, Langmuir 28 (4) (2012) 2137–2144.
[48] E. Hanke, U. Schulz, U. Kaatze, Molecular interactions in poly(ethylene glycol)-water mixtures at various temperatures: Density and isentropic compressibility study, ChemPhysChem 8 (4) (2007) 553–560.
[49] F. Beiranvand, H. Najibi, B. Hashemi Shahraki, Experimental Measurement of Equilibrium Surface Tension of an Aqueous Solution of Polyethylene Glycol and a Surfactant, Chem. Eng. Res. Artic. Iran. J. Oil Gas Sci. Technol. 9 (3) (2020) 26–43.
[50] M. Lim, M. Ashokkumar, Y. Son, The effects of liquid height/volume, initial concentration of reactant and acoustic power on sonochemical oxidation, Ultrason. Sonochem. 21 (6) (2014) 1988–1993.
[51] T. Van Gerven, A. Stankiewicz, Structure, energy, synergy, time-the fundamentals of process intensification, Ind. Eng. Chem. Res. 48 (5) (2009) 2465–2474.
[52] O. Louisnard, I. Garcia-Vargas, Simulation of Sonoreators Accounting For Dissipated power, First Edit, Elsevier Ltd., 2022.
[53] N.C. Eddingsaas, K.S. Suslick, Evidence for a plasma core during multibubble sonoluminescence in sulfuric acid, J. Am. Chem. Soc. 129 (13) (2007) 3838–3839.
[54] O. Louisnard, A simple model of ultrasound propagation in a cavitating liquid. Part I: Theory, nonlinear attenuation and traveling wave generation, Ultrason. Sonochem. 19 (1) (Jan. 2012) 56–65.
[55] A. Moussatov, C. Granger, B. Dubus, Cone-like bubble formation in ultrasonic cavitation field, Ultrason. Sonochem. 10 (4–5) (2003) 191–195.